

# Geophysical Research Letters<sup>®</sup>

## RESEARCH LETTER

10.1029/2025GL115834

### Key Points:

- The downward frequency chirping between rising-tone EMIC wave subpackets is demonstrated
- Subpacket formation in EMIC waves is associated with the oscillation of proton holes in gyrophase space driven by cyclotron resonance
- The energy transfer through cyclotron resonance is maximized at subpacket peaks, different from that associated with Landau resonance

### Supporting Information:

Supporting Information may be found in the online version of this article.

### Correspondence to:

H. Chen and X. Wang,  
[huayue\\_chen@foxmail.com](mailto:huayue_chen@foxmail.com);  
[wangxue@auburn.edu](mailto:wangxue@auburn.edu)

### Citation:

Chen, H., Wang, X., Lin, Y., Zhao, H., Wang, C.-P., Li, X., et al. (2025). Nonlinear proton dynamics in the formation of rising-tone EMIC wave subpackets. *Geophysical Research Letters*, 52, e2025GL115834. <https://doi.org/10.1029/2025GL115834>

Received 9 MAR 2025

Accepted 16 MAY 2025

## Nonlinear Proton Dynamics in the Formation of Rising-Tone EMIC Wave Subpackets



Huayue Chen<sup>1</sup> , Xueyi Wang<sup>1</sup> , Yu Lin<sup>1</sup> , Hong Zhao<sup>1</sup> , Chih-Ping Wang<sup>2</sup> , Xinmin Li<sup>3</sup> , Shujie Gu<sup>4</sup> , Yoshiharu Omura<sup>5</sup> , Lunjin Chen<sup>4</sup> , Xiaolei Li<sup>1</sup> , and Yi-Kai Hsieh<sup>5</sup>

<sup>1</sup>Department of Physics, Auburn University, Auburn, AL, USA, <sup>2</sup>Department of Atmospheric and Oceanic Sciences, University of California, Los Angeles, Los Angeles, CA, USA, <sup>3</sup>Boston University, Boston, MA, USA, <sup>4</sup>William B. Hanson Center for Space Sciences, University of Texas at Dallas, Richardson, TX, USA, <sup>5</sup>Research Institute for Sustainable Humanosphere, Kyoto University, Kyoto, Japan

**Abstract** Electromagnetic ion cyclotron (EMIC) waves are commonly observed in the Earth's magnetosphere and play a significant role in regulating relativistic electron fluxes. The waveform of EMIC waves comprises amplitude-modulated wave packets, known as "subpackets." Despite their prevalence, the underlying physics and associated particle dynamics for subpacket formation remain poorly understood. In this study, using Van Allen Probe A observations, we present several rising-tone EMIC wave events to reveal the downward frequency chirping between adjacent subpackets. By performing a hybrid simulation, we demonstrate for the first time that these wave properties are associated with the oscillation of proton holes in the wave gyrophase space induced by cyclotron resonance. The oscillation modulates the energy transfer between waves and particles, establishing a direct link between subpacket formation in cyclotron waves and nonlinear wave-particle interactions. This new understanding advances our knowledge of subpacket formation in general and its broader implications in space plasma physics.

**Plain Language Summary** Electromagnetic ion cyclotron (EMIC) waves, driven by proton cyclotron resonance instability, play a crucial role in the loss of relativistic electrons from radiation belts. The waveform of EMIC waves generally consists of wave packets with modulated amplitudes, known as "subpackets." This study examines the physical mechanism underlying subpacket formation and the associated proton dynamics. Through the analysis of three EMIC wave events observed by Van Allen Probe A, we find that while the wave spectrum exhibits an overall increasing frequency trend, the frequency between adjacent subpackets subtly decreases. Using a numerical simulation, we demonstrate that these wave properties are associated with the proton holes induced by cyclotron resonance. The proton holes oscillate in size during subpacket formation, determining the energy transfer process in nonlinear wave-particle interactions. In light of earlier reports of electron hole oscillations in chorus wave subpackets, our results confirm that the oscillation of phase-space holes is a general characteristic in subpacket formation driven by nonlinear wave-particle interactions through cyclotron resonance.

## 1. Introduction

Electromagnetic ion cyclotron (EMIC) waves are naturally occurring in the Earth's magnetosphere and are categorized as Pc1-Pc2 geomagnetic pulsations, with frequencies ranging from 0.1 to 5 Hz (Bortnik et al., 2007; L. Chen et al., 2016; H. Chen et al., 2020; Horne & Thorne, 1994; Min et al., 2012; Usanova et al., 2012). These waves play a crucial role in modulating particle fluxes in the radiation belts (L. Chen et al., 2019; Grach & Demekhov, 2020; Miyoshi et al., 2008; Nakamura et al., 2022; Omura & Zhao, 2013; Summers & Thorne, 2003), thereby influencing spacecraft operations (Chu et al., 2021; Meredith et al., 2024) and space weather (Green & Kivelson, 2004; Reeves et al., 2013).

The waveform of EMIC waves typically comprises a series of wave packets with modulated amplitudes on timescales ranging from tens of seconds to several minutes (Mursula et al., 2001; Usanova et al., 2010; Ukhorskiy et al., 2010; X. An et al., 2024). These modulated structures, commonly referred to as "subpackets" (Kubota et al., 2015; Nakamura et al., 2015; Ojha et al., 2021), are of particular scientific interest due to their role in the rapid loss of sub-MeV to ~MeV electrons from the radiation belts (X. An et al., 2024; L. Chen et al., 2016). The formation of subpackets has been previously attributed to the superposition of EMIC waves with Pc5 ultra-low-frequency (ULF) waves (Loto'aniu et al., 2009; Mursula et al., 2001). More recently, nonlinear wave-particle

© 2025 The Author(s).

This is an open access article under the terms of the Creative Commons Attribution-NonCommercial License, which permits use, distribution and reproduction in any medium, provided the original work is properly cited and is not used for commercial purposes.

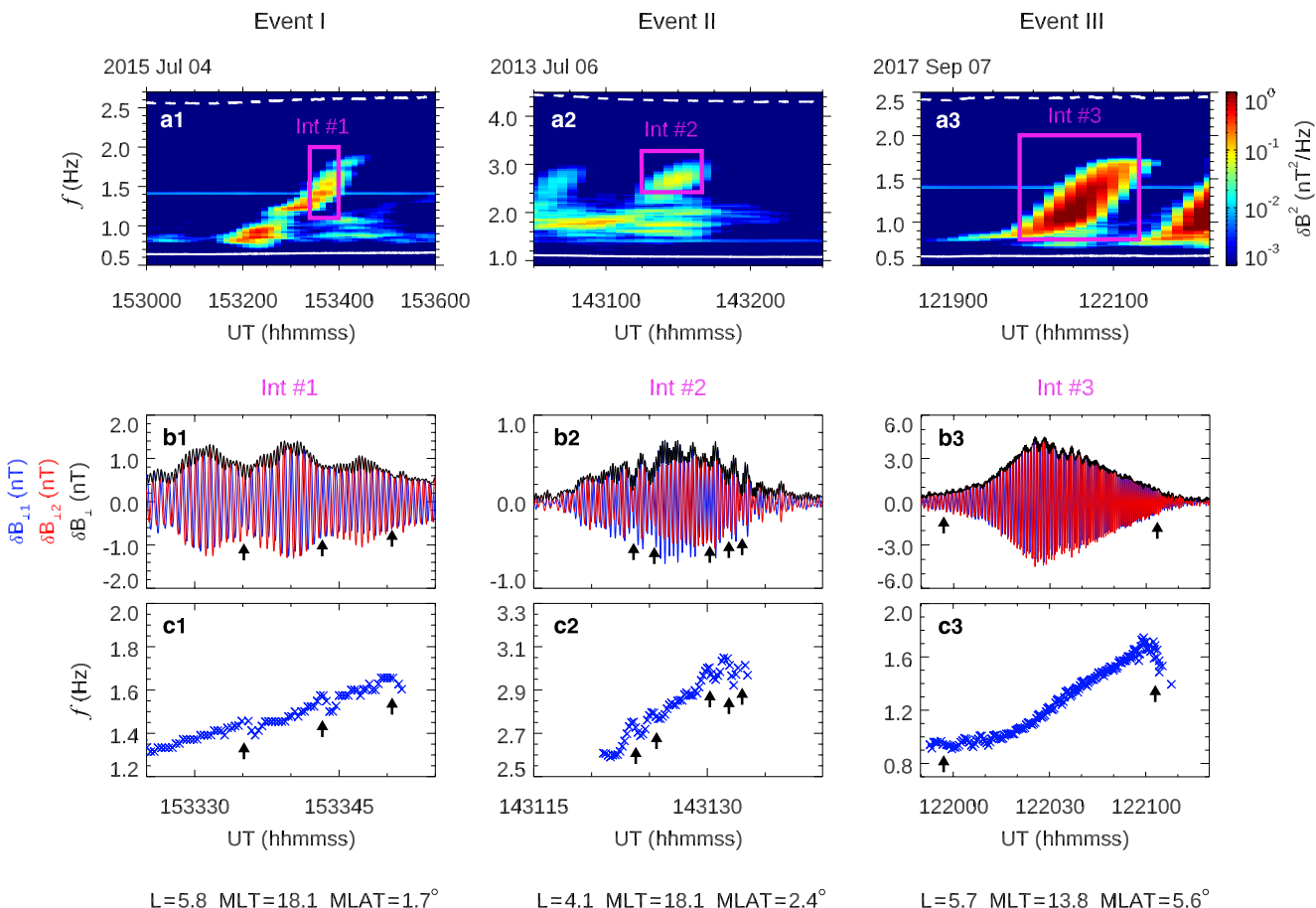


**Figure 1.** Three rising-tone EMIC wave events observed by Van Allen Probe A in the inner magnetosphere. The columns from left to right correspond to Event I detected on 04 July 2015, Event II on 06 July 2013, and Event III on 07 September 2017. (a1–a3) Wave spectra of  $\delta B$ , with magenta boxes indicating the time intervals (Int #1–#3) and corresponding frequency ranges of interest (Int #1: 1.2–2.0 Hz; Int #2: 2.5–3.3 Hz; Int #3: 0.8–2.0 Hz). The white dashed and solid curves represent the proton gyrofrequency  $f_{cp}$  and the helium gyrofrequency  $f_{He^+}$ , respectively. (b1–b3) Zoom-in plots of magnetic field perturbations, including  $\delta B_{11}$  (blue),  $\delta B_{12}$  (red), and  $\delta B$  (black). (c1–c3) Instantaneous frequency within the intervals Int #1–#3. To minimize noise interference, only instantaneous frequencies corresponding to wave amplitudes exceeding a threshold are shown. The  $\delta B$  threshold is set to 0.5 nT for Int #1 and Int #3, and 0.3 nT for Int #2 due to weak wave power. Black arrows in panels (b1–b3) denote the subpacket troughs, and those in panels (c1–c3) denote the downward frequency chirping.

interactions have been proposed as a critical mechanism in the formation of rising-tone EMIC wave subpackets, where the frequency increases with time, with evidence showing that wave amplitudes are above the thresholds required for nonlinear processes (Nakamura et al., 2015; Ojha et al., 2021; Shoji & Omura, 2013). Although rising-tone EMIC wave subpackets are frequently observed (Z. An et al., 2024; Nakamura et al., 2016; Y. Wang et al., 2023), the underlying nonlinear physics and associated particle dynamics for subpacket formation remain poorly understood.

In this study, using observations from Van Allen Probe A, we investigate the wave properties of rising-tone EMIC wave subpackets. We also perform a hybrid simulation in the dipole magnetic field to examine the physical processes and the nonlinear proton dynamics during subpacket formation. It is found that the oscillation of the proton phase-space holes plays an important role in subpacket formation and determines the energy transfer between waves and particles.

## 2. Observational Results

The Van Allen Probes mission consists of two identical satellites, A and B (Kessel et al., 2012). The onboard Electric and Magnetic Field Instrument and Integrated Science (EMFISIS; Wygant et al., 2013) instrument provides magnetic field measurements sampled at 64 Hz rates. The wave spectrum is derived through fast Fourier transform (FFT) algorithm. The local background magnetic field  $B_0$  is obtained by applying a 10-s smoothing to

the magnetic field data, while the equatorial background magnetic field  $B_{e0}$  is estimated using the Earth's dipole magnetic field model.

Figure 1 presents three rising-tone EMIC wave events observed by Van Allen Probe A in the inner magnetosphere at L-shell ( $L = 4\text{--}6$ , labeled as Events I–III (from left to right). Figures 1a1–1a3 illustrate the spectrum of  $\delta B$  for these three events, respectively. The wave amplitude is defined as  $\delta B = \sqrt{\delta B_{\perp 1}^2 + \delta B_{\perp 2}^2}$ , where the “ $\perp 1$ ” direction in observational data is defined as the cross product of the local background magnetic field  $B_0$  and the sunward direction, and the “ $\perp 2$ ” direction is determined to complete the orthogonal triad. Strong wave power is seen at frequencies between the helium gyrofrequency  $f_{cHe^+}$  and the proton gyrofrequency  $f_{cp}$  (where  $f_{cHe^+} = eB_{e0}/(2\pi m_{He^+})$  and  $f_{cp} = eB_{e0}/(2\pi m_p)$ ,  $e$  is the elementary charge, and  $m_{He^+}$  and  $m_p$  are the helium and proton masses, respectively), indicating that the waves belong to the proton band. The wave spectra exhibit upward frequency chirping. The average chirping rates for the three events are  $\Gamma = \partial f / \partial t = 2.8 \times 10^{-2}, 8.0 \times 10^{-2}$ , and  $6.3 \times 10^{-2}$  Hz/s, corresponding to the normalized chirping rates of  $\partial \omega / \partial t = 7.6 \times 10^{-4}, 7.2 \times 10^{-4}$ , and  $2.1 \times 10^{-3} \Omega_{p0}^2$ , where  $\Omega_{p0} = 2\pi f_{cp}$ . The background plasma parameters for the three events are shown in Figure S1 in Supporting Information S1. For each spectrum, we select one time interval (Int #1–#3), highlighted by a magenta box, to analyze the frequency chirping. Figure 1b1–1b3 show the temporal evolution of  $\delta B_{\perp 1}$  (blue),  $\delta B_{\perp 2}$  (red), and  $\delta B$  (black) within these intervals. Multiple subpackets are observed in Int #1 and Int #2, with the subpacket troughs marked by black arrows. Int #3 contains only a single subpacket, constituting the rising-tone element depicted in Figure 1a3, with black arrows indicating the subpacket boundaries. Figures 1c1–1c3 show that the instantaneous frequency, quantified based on the zero-crossings of  $\delta B_{\perp 1}$ , increases with time, revealing an overall upward chirping trend consistent with the rising-tone spectrum. However, subtle downward chirping is seen at subpacket troughs, as indicated by the black arrows in Figures 1c1–1c3. The downward chirping inside the upward chirping spectrum of EMIC wave subpackets is similar to the chirping characteristics of chorus wave subpackets in the Earth's magnetosphere (H. Chen et al., 2023; Santolík et al., 2014; Tsurutani et al., 2020; X. Wang et al., 2024; Zhang et al., 2020).

To investigate proton dynamics during subpacket formation, we perform a one-dimensional (1-D) hybrid simulation in the dipole magnetic field. The simulation results are further compared with the nonlinear theory.

### 3. Hybrid Simulation in a Dipole Magnetic Field

#### 3.1. Simulation Model

We perform a 1-D hybrid simulation using the general curvilinear plasma simulation code (GCPIC) model in a dipole field (Kang et al., 2021; X. Wang et al., 2024). The simulation model solves Maxwell's equations and particle motions in dipole coordinates, where particle trajectories are calculated by advancing their three-dimensional (3-D) velocities and positions in the background dipole magnetic fields plus perturbed electromagnetic fields. The simulation domain is along the magnetic field line at  $L = 6$ , spanning a magnetic latitude ( $\lambda$ ) range from  $\sim -30^\circ$  to  $\sim 30^\circ$ . In this model, protons are the sole ion species and are treated kinetically as particles, while electrons are modeled as a resistive fluid to maintain charge neutrality. Reflective boundary conditions are applied to both particles and wave fields.

Plasma parameters used in the simulation are derived from three events in Figure 1, combined with typical values at  $L \sim 6$ . The background magnetic field and plasma density at the magnetic equator are  $B_{e0} = 144.4$  nT and  $n_{e0} = 20.0 \text{ cm}^{-3}$  (Denton et al., 2004), yielding an equatorial Alfvén speed of  $V_{A0} = B_{e0}/\sqrt{\mu_0 n_{e0} m_p} = 704.6 \text{ km/s}$ , where  $\mu_0$  is the vacuum permeability. The plasma system includes both hot and cold protons, with equatorial number densities of 0.05  $n_{e0}$  and 0.95  $n_{e0}$ , respectively. The hot protons follow a subtracted Maxwellian distribution (H. Chen et al., 2023; Omura, 2021; Zenitani & Nakano, 2023), given by:

$$f(u_{||}, u_{\perp}) = \frac{n_{heq}}{(2\pi)^{3/2} U_{||} U_{\perp}^2 (1 - \rho\beta)} \exp\left(-\frac{u_{||}^2}{2U_{||}^2}\right) \cdot \left[ \exp\left(-\frac{u_{\perp}^2}{2U_{\perp}^2}\right) - \rho \exp\left(-\frac{u_{\perp}^2}{2\beta U_{\perp}^2}\right) \right], \quad (1)$$

where  $\rho = 1$  and  $\beta = 0.3$ . Here,  $n_{heq}$  denotes the equatorial number density of hot protons,  $U_{||}$  and  $U_{\perp}$  represent the parallel and perpendicular thermal momenta, and  $u_{||}$  and  $u_{\perp}$  are the parallel and perpendicular momenta,

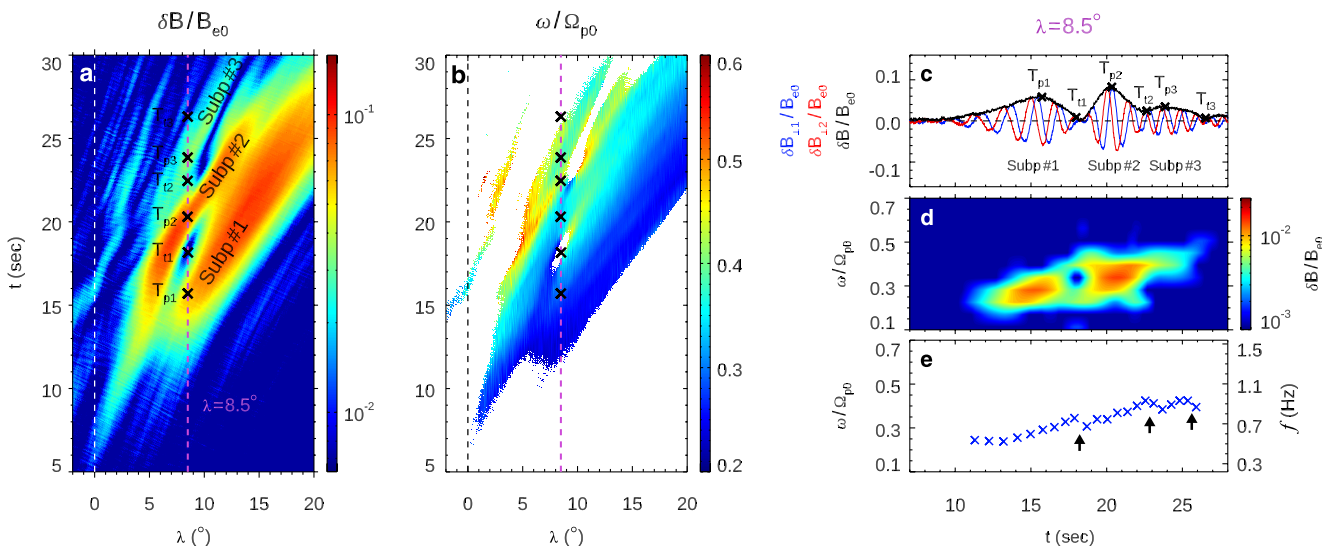


**Figure 2.** Simulation results of forward-propagating EMIC waves. (a) Normalized wave amplitude  $\delta B/B_{e0}$  and (b) normalized instantaneous frequency  $\omega/\Omega_{p0}$  in the  $\lambda$ - $t$  plane, with the white or black dotted lines representing  $\lambda = 0^\circ$  and the magenta dashed lines indicating  $\lambda = 8.5^\circ$ . Three subpackets are labeled as “Subp #1–#3.” Six time points ( $T_{p1} = 15.80$  s,  $T_{t1} = 18.00$  s,  $T_{p2} = 20.22$  s,  $T_{t2} = 22.58$  s,  $T_{p3} = 23.92$  s, and  $T_{t3} = 26.23$  s) are marked by black crosses at  $\lambda = 8.5^\circ$ . (c–e) Wave properties at  $\lambda = 8.5^\circ$ . (c) Temporal evolution of  $\delta B_{\perp 1}/B_{e0}$  (blue),  $\delta B_{\perp 2}/B_{e0}$  (red), and  $\delta B/B_{e0}$  (black), with the black dashed line indicating the zero value. Six time points ( $T_{p1}$ – $T_{p3}$  and  $T_{t1}$ – $T_{t3}$ ) are indicated by black crosses. (d) The  $\omega$ - $t$  spectrum of  $\delta B/B_{e0}$ . (e) The normalized instantaneous frequency  $\omega/\Omega_{p0}$  and the instantaneous frequency  $f$  in Hz. Black arrows in panel (e) point at the downward frequency chirping at subpacket troughs.

respectively. The normalized parallel thermal momentum is  $U_{th\parallel}/V_{A0} = 1.97$ , corresponding to a parallel temperature of 20 keV (Kim et al., 2024). The temperature anisotropy is given by  $U_{th\perp}^2/U_{th\parallel}^2 = 2.0$  (Yue et al., 2019). The cold protons follow a Maxwellian distribution with a temperature of 10 eV.

### 3.2. Simulation Results

Figure 2a illustrates the normalized amplitude  $\delta B/B_{e0}$  of forward-propagating EMIC waves in the  $\lambda$ - $t$  plane, filtered in a frequency range of 0.1–0.9  $\Omega_{p0}$ . Figure 2b shows the corresponding instantaneous frequency  $\omega/\Omega_{p0}$ , evaluated where  $\delta B/B_{e0}$  exceeds 0.02. These waves are self-consistently excited by hot protons, and the forward- and backward-propagating branches are separated based on helicity, following the method in Terasawa et al. (1986). A series of wave packets with weak amplitudes of  $\delta B/B_{e0} \sim 10^{-2}$  initially appear in a region below the magnetic equator, driven by the counterstreaming resonant protons modulated in gyrophase. As the waves propagate across the magnetic equator and toward higher latitudes, their amplitudes grow to  $\delta B/B_{e0} \sim 10^{-1}$  through nonlinear interactions with incoming resonant protons. The waves fall within the proton band. Their frequencies exhibit an overall upward trend, with subtle decreases at subpacket troughs, as more clearly illustrated in the scatter plot in Figure 2e. When observed at a fixed position, the wave packets manifest as rising-tone emissions with subpacket structures.

Figure 2c presents the temporal evolution of normalized wave magnetic fields  $\delta B_{\perp 1}/B_{e0}$  and  $\delta B_{\perp 2}/B_{e0}$ , and the wave amplitude  $\delta B/B_{e0}$  at  $\lambda = 8.5^\circ$ . In the simulation data, “ $\perp 1$ ” represents the L-shell direction, and “ $\perp 2$ ” corresponds to the azimuthal direction. The waveform consists of three subpackets, labeled as “Subp #1–#3.” Figures 2d and 2e show the wave spectrum and the instantaneous frequency, respectively. The spectrum exhibits a rising-tone chirping, with the frequency increasing from  $\sim 0.22 \Omega_{p0}$  ( $\sim 0.5$  Hz) at  $t \sim 11$  s to  $\sim 0.45 \Omega_{p0}$  ( $\sim 1.0$  Hz) at  $t \sim 26$  s, corresponding to a normalized chirping rate of  $\Gamma = \partial\omega/\partial t = 1.1 \times 10^{-3} \Omega_{p0}^2$  ( $\partial f/\partial t = 3.3 \times 10^{-2}$  Hz/s). The chirping rate in the simulation is comparable to those of the three events shown in Figure 1, as well as to the typical values of  $\Gamma \sim 10^{-3}$ – $10^{-2} \Omega_{p0}^2$  reported in the observational study of Y. Wang et al. (2023). The instantaneous frequency also demonstrates an overall upward chirping. However, slight downward chirping signals are seen between adjacent subpackets (indicated by the black arrows in Figure 2e), coinciding with the local minima in wave amplitude. Therefore, the characteristics of the simulated frequency chirping in subpackets are consistent with the observations shown in Figure 1.

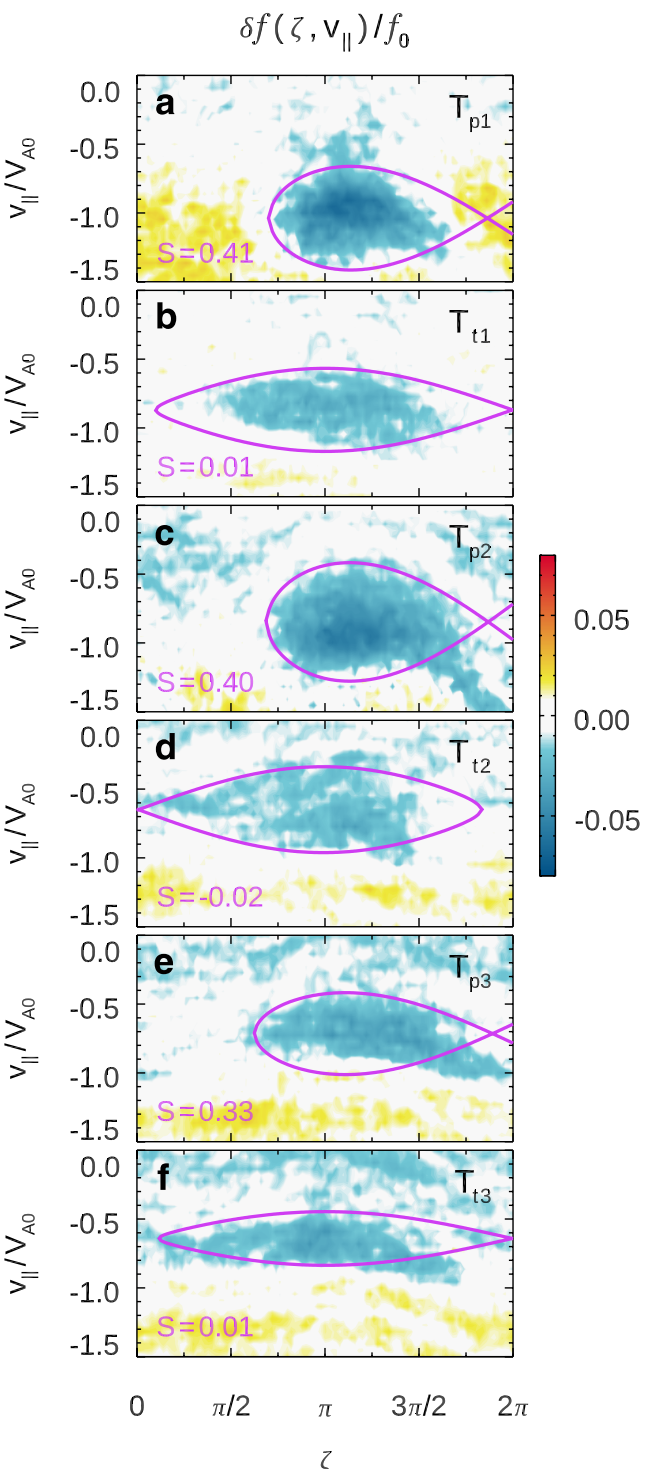


**Figure 3.** Evolution of phase space density of hot protons in the simulation. Disturbed phase space density  $\delta f = f - f_0$  in the  $\zeta - v_{\parallel}$  plane at the time points: (a)  $T_{p1}$ , (b)  $T_{t1}$ , (c)  $T_{p2}$ , (d)  $T_{t2}$ , (e)  $T_{p3}$ , and (f)  $T_{t3}$ . In each panel, the proton hole envelope is enclosed by a magenta curve, with the corresponding inhomogeneity factor  $S$  indicated.

We select six time points at  $\lambda = 8.5^\circ$ , two points for each of the three subpackets (indicated by the black crosses in Figures 2a–2c), to investigate the nonlinear proton dynamics during subpacket formation. The time points  $T_{p1}$ ,  $T_{p2}$ , and  $T_{p3}$  represent the subpacket peaks, which correspond to the local maxima of wave amplitude. While  $T_{t1}$ ,  $T_{t2}$ , and  $T_{t3}$  denote to the subpacket troughs, where the wave amplitude reaches its local minima.

A proton hole is a region with relatively lower phase space density as compared to surrounding areas, formed due to nonlinear wave-particle interactions through cyclotron resonance. At time point  $T_{p1}$ , the cyclotron resonant velocity is  $v_c = (\omega - \Omega_p)/k = -1.04V_{A0}$ , calculated using the wave frequency of  $\omega/\Omega_{p0} = 0.29$  and the wave number of  $kV_{A0}/\Omega_{p0} = 0.64$ , where  $\Omega_p = eB_0/m_p$  is the local proton gyrofrequency. Figure 3a illustrates the disturbed phase space density  $\delta f(\zeta, v_{\parallel}) = f - f_0$  of hot protons at  $\lambda = 8.5^\circ$ , where  $f$  represents the instantaneous distribution, at  $T_{p1}$ ,  $f_0$  represents the initial distribution,  $\zeta$  denotes the gyrophase angle between the perpendicular velocity  $v_{\perp}$  of protons and the disturbed magnetic field  $\delta B$  of EMIC waves, and  $v_{\parallel}$  is the parallel velocity of protons. Around  $v_c$ , a proton hole, as indicated by negative  $\delta f$ , forms within the range of  $\zeta \approx \pi/2 - 2\pi$ . This proton hole is consistent with the classical proton hole topology described by the nonlinear theory (Omura et al., 2010).

Figures 3b–3f show the  $\delta f(\zeta, v_{\parallel})$  at other time points, where the proton holes are seen at both subpacket peaks and troughs. The central position of proton holes in  $v_{\parallel}$  is around  $v_c$ , with  $|v_c|$  decreasing with time (see Table S1 in Supporting Information S1) due to the upward frequency chirping (Figure 2d). Meanwhile, the central position in  $\zeta$  oscillates with a period of  $\sim 4$  s, corresponding to the timescale of subpackets. At subpacket peaks (Figures 3a, 3c, and 3e), the proton holes are located within  $\zeta \approx \pi/2 - 2\pi$ , while they expand to  $\zeta \approx 0 - 2\pi$  and become nearly symmetric around  $\zeta = \pi$  at subpacket troughs (Figures 3b, 3d, and 3f).

Based on the nonlinear theory (Omura et al., 2010), the envelope of a proton hole in the wave gyrophase space satisfies:

$$k^2(v_{\parallel} - v_c)^2 + 2\omega_{tr}^2(\cos \zeta - S\zeta) = C, \quad (2)$$

where  $\omega_{tr}^2 = kv_{\perp}\Omega_w$  with  $\Omega_w = e\delta B/m_p$ ,  $S$  is the inhomogeneity factor, and  $C$  is a constant. The parameters of the wave properties ( $\omega$ ,  $k$ ,  $\delta B$ , and  $v_c$ ) are listed in Table S1 in Supporting Information S1, and  $v_{\perp}$  is set to  $2 V_{A0}$ . In Figure 3, the proton hole envelope is fitted with a magenta curve at each time point. The corresponding  $S$  values at the six time points are determined from Equation 2 as 0.41, 0.01, 0.40,  $-0.02$ , 0.33, and 0.01, respectively. These results indicate that  $S$  is  $\sim 0.4$  at subpacket peaks while is  $\sim 0$  at subpacket troughs. Therefore, the  $S$  value is not a constant, which is contrary to the assumption of  $S$  being a constant commonly used in previous studies.

The inhomogeneity factor can be derived not only from the particle dynamics but also from the wave properties in an inhomogeneous plasma system. The theoretical inhomogeneity factor  $S_{th}$  is defined as (Shoji & Omura, 2017; Omura et al., 2010):

$$S_{th} = \frac{1}{s_0\omega\Omega_w} \left( s_1 \frac{\partial\omega}{\partial t} + v_p s_2 \frac{\partial\Omega_p}{\partial h} \right), \quad (3)$$

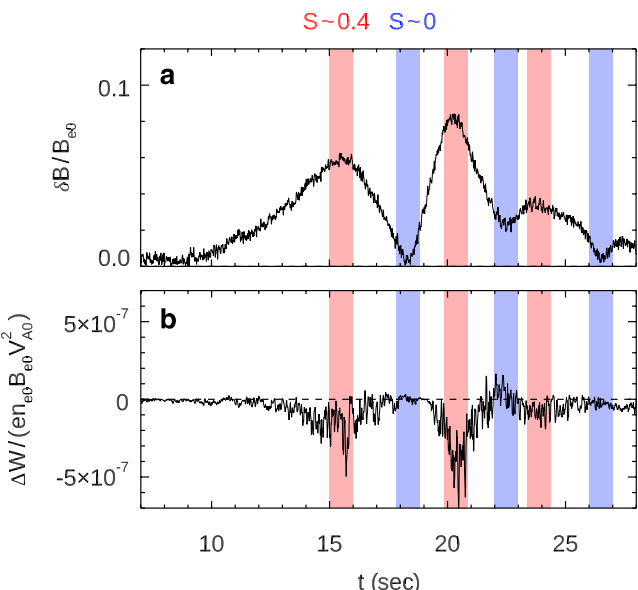


**Figure 4.** Simulated energy transfer between waves and hot protons at  $\lambda = 8.5^\circ$ . Temporal evolution of (a) normalized wave amplitude  $\delta B / B_{e0}$  and (b) energy transfer  $\Delta W$ . The red-shaded regions indicate subpacket peaks, corresponding to  $S \sim 0.4$ , while the blue-shaded regions denote subpacket troughs with  $S \sim 0$ . In panel (b), the black dotted line represents the zero value.

The resulting  $R^2 = 0.89$  suggests that  $S_{th}$  is consistent with the  $S$  derived from proton holes. At subpacket peaks, both the frequency chirping term (with a mean value of  $\partial\omega/\partial t = 3.2 \times 10^{-3}\Omega_{p0}^2$ ) and the field gradient term contribute to positive inhomogeneity. While at subpacket troughs, the two terms have comparable magnitudes but opposite signs (with a mean value of  $\partial\omega/\partial t = -1.9 \times 10^{-3}\Omega_{p0}^2$ ), leading to  $S_{th} \sim 0$ . Therefore, the distinct frequency chirping characteristics at different stages of subpacket formation is associated with the nonlinear wave-particle interactions.

#### 4. Discussions

The nonlinear theory proposes that inhomogeneity factor determines the energy transfer process between waves and particles, with the maximum energy transfer at  $S \sim 0.4$  for rising-tone EMIC waves (Omura et al., 2010). We can quantify the energy transfer  $\Delta W$  in the simulation, defined as:

$$\Delta W = \int_0^\infty \int_0^{2\pi} \int_{-\infty}^\infty f(u_{||}, \zeta, u_\perp) ev \cdot \delta Eu_\perp du_{||} d\zeta du_\perp, \quad (7)$$

where  $u = \gamma v$  is the momentum,  $\gamma$  is the relativistic factor, and  $f(u_{||}, \zeta, u_\perp)$  represents the phase space density of hot protons. A negative (positive) value of  $\Delta W$  indicates energy transfer from particles to waves (from waves to particles). Figure 4b shows the temporal evolution of  $\Delta W$  at  $\lambda = 8.5^\circ$ , with the wave amplitude  $\delta B / B_{e0}$  overlaid in Figure 4a for reference. Throughout the subpacket formation,  $\Delta W$  is primarily negative, indicating a net energy transfer from particles to waves, even as the amplitude decreases from subpacket peaks to subpacket troughs. Specifically,  $|\Delta W|$  reaches its maximum at subpacket peaks (red-shaded regions), consistent with the nonlinear theory, while is  $\sim 0$  at subpacket troughs (blue-shaded regions). The above correlation between the simulated  $\Delta W$  values and the subpackets is consistent with a previous observational study using Time History of Events and Macroscale Interactions during Substorms (THEMIS) data (Shoji et al., 2017), in which they found that  $|\Delta W|$  is minimal at EMIC wave subpacket troughs.

The variation of energy transfer  $\Delta W$  is attributed to the evolution of particle dynamics in the wave gyrophase space. At subpacket peaks, the proton holes are located around  $\zeta = 3\pi/2$  (Figures 3a, 3c, and 3e), corresponding to

where

$$s_0 = \frac{v_\perp}{v_p}, \quad (4)$$

$$s_1 = \left(1 - \frac{v_c}{v_g}\right)^2, \quad (5)$$

and

$$s_2 = \left(\frac{v_\perp^2}{2v_p^2} + \frac{v_c^2}{v_p v_g} - \frac{v_c^2}{2v_p^2}\right) \frac{\omega}{\Omega_p} - \frac{v_c}{v_p}. \quad (6)$$

Here,  $v_p$  and  $v_g$  represent the wave phase velocity and group velocity, respectively, and  $h$  is the distance along a field line from the magnetic equator. The  $S_{th}$  consists of two terms: the frequency chirping term, which depends on  $\partial\omega/\partial t$ , and the field gradient term, which depends on  $\partial\Omega_p/\partial h$  (or  $\partial B_0/\partial h$ ). At  $\lambda = 8.5^\circ$ ,  $\partial B_0/\partial h$  is estimated as  $3.7 \times 10^{-3} B_{e0} \Omega_{p0}/V_{A0}$  (see Figure S2 in Supporting Information S1). Using the chirping rates obtained from the simulation, we evaluate  $S_{th}$  during different stages of subpackets:  $S_{th} = 0.35, 0.04, 0.30, -0.03, 0.40$ , and  $0.03$ , respectively. The fitting coefficient is calculated as  $R^2 = 1 - \text{SSE/SST}$ , where SSE is the sum of squared differences between  $S$  and  $S_{th}$ , and SST is the sum of squared differences between  $S_{th}$  and their mean. A value of  $R^2$  close to 1 indicates a reliable fit.

the gyrophase angle of wave electric field  $\delta E$ , which results in  $\Delta W$  being significantly negative. While at subpacket troughs, the proton holes become nearly symmetric around  $\zeta = \pi$  (Figures 3b, 3d, and 3f), leading to  $\Delta W \sim 0$ .

In this study, EMIC wave subpackets are driven by nonlinear wave-particle interactions through cyclotron resonance. The energy transfer process via cyclotron resonance is distinctly different from that associated with Landau resonance. During the nonlinear stage of Landau resonance, energy conservation remains between waves and particles, leading to no energy transfer at subpacket peaks and troughs (O'Neil, 1965). In contrast, during the subpacket formation resulting from cyclotron resonance, energy transfer is maximized at subpacket peaks.

The energy transfer  $\Delta W$  determines the full-time derivative of  $\delta B$  along subpacket propagation, denoted as  $d(\delta B)/dt$ . While the temporal evolution of  $\delta B$  at a specific position corresponds to the partial derivative  $\partial(\delta B)/\partial t$  (Figures 1d–1f and 2c). The difference between  $d(\delta B)/dt$  and  $\partial(\delta B)/\partial t$  is the spatial convection term,  $\partial(\delta B)/\partial h$ , which describes the spatial variation of  $\delta B$  (H. Chen et al., 2024; X. Wang et al., 2024). However, to fully understand subpacket formation, a detailed analysis of phase-trapping and phase-bunching particles is required, which will be addressed in future work.

Nonlinear wave-particle interactions in subpacket formation for both chorus waves and EMIC waves are similar. In the gyrophase of chorus waves, electron holes form due to cyclotron resonance (H. Chen et al., 2024) and they oscillate in size at different stages of subpacket formation (X. Wang et al., 2024). The corresponding inhomogeneity factor  $S$  changes from  $\sim -0.4$  at subpacket peaks to  $\sim 0$  at subpacket troughs (X. Wang et al., 2024). In the gyrophase of EMIC waves, proton holes are also generated through cyclotron resonance and undergo similar oscillations. However, the  $S$  value is  $\sim 0.4$  at subpacket peaks due to the opposite charge of particles. Therefore, the oscillation of phase-space holes is a general characteristic in subpacket formation driven by nonlinear wave-particle interactions through cyclotron resonance.

In this study, we analyze three EMIC wave subpacket events observed by Van Allen Probe A. While these events provide valuable insight into wave properties, a broader data set is needed for more general conclusions. Besides, Van Allen Probes cannot measure particle data in the gyrophase. To address these limitations, we plan to perform a statistical analysis using Magnetospheric Multiscale Mission (MMS) data, which provides high time-resolution ion measurements suitable for such analysis. This will be pursued in future work. In the simulation model, ion population includes only protons; heavy ions such as  $\text{He}^+$  or  $\text{O}^+$  are not considered. Although heavy ions can modify the EMIC wave dispersion relation (Denton et al., 2014) and can undergo resonant heating (H. Chen et al., 2018), their impact is beyond the scope of this study and will also be explored in future work.

## 5. Summary

We investigated the wave properties of rising-tone EMIC wave subpackets using observations from Van Allen Probe A. We also conducted a hybrid simulation of EMIC waves in the dipole field and analyzed the nonlinear proton dynamics in the formation of subpackets. The main conclusions are as follows:

1. Although the overall trend in EMIC wave spectrum shows rising-tone chirping, the frequency between adjacent subpackets is subtle downward chirping, as demonstrated by both satellite observations and simulation results.
2. The proton holes in wave gyrophase space, induced by cyclotron resonance, oscillate in size with time during subpacket formation. The inhomogeneity factor  $S$  changes accordingly, with  $S \sim 0.4$  at subpacket peaks while  $S \sim 0$  at subpacket troughs.
3. The evolution of proton holes determines the energy transfer between waves and protons, with maximum energy transfer from protons to waves occurring at subpacket peaks and negligible transfer at subpacket troughs.

## Data Availability Statement

The data from Van Allen Probe A are from <https://spdf.gsfc.nasa.gov/pub/data/rbsp/rbspa/>. The simulation data are available at H. Chen (2025).

**Acknowledgments**

This work was supported by the NASA Grants 80NSSC24K0174, 80NSSC21K1688, 80NSSC21K1679, 80NSSC23K0086, 80NSSC22K1012, and the NSF Grants AGS-2131012, AGS-2247759, and AGS-2224109. Work at UTD supported by the NASA Grant 80NSSC24K0558 and the NSF Grant AGS-2225121. YO and YH were supported by JSPS KAKENHI Grants JP20H01960 and JP23H05429. Computer resources are provided by NASA NAS Division. We thank the entire Van Allen Probes team and instrument principal investigators for providing and calibrating data.

**References**

- An, X., Artemyev, A., Angelopoulos, V., Zhang, X.-J., Mourenas, D., Bortnik, J., & Shi, X. (2024). Nonresonant scattering of energetic electrons by electromagnetic ion cyclotron waves: Spacecraft observations and theoretical framework. *Journal of Geophysical Research: Space Physics*, 129(3), e2023JA031863. <https://doi.org/10.1029/2023JA031863>
- An, Z., Tao, X., Zonca, F., & Chen, L. (2024). Frequency chirping of electromagnetic ion cyclotron waves in Earth's magnetosphere. *Geophysical Research Letters*, 51(4), e2023GL106456. <https://doi.org/10.1029/2023GL106456>
- Bortnik, J., Cutler, J. W., Dinson, C., & Bleier, T. E. (2007). An automatic wave detection algorithm applied to Pc1 pulsations. *Journal of Geophysical Research*, 112(A4), A04204. <https://doi.org/10.1029/2006JA011900>
- Chen, H. (2025). Database of "nonlinear proton dynamics in the formation of rising-tone EMIC wave subpackets" [Dataset]. *Zenodo*. <https://zenodo.org/records/15476383>
- Chen, H., Gao, X., Lu, Q., Tsurutani, B. T., & Wang, S. (2020). Statistical evidence for EMIC wave excitation driven by substorm injection and enhanced solar wind pressure in the Earth's magnetosphere: Two different EMIC wave sources. *Geophysical Research Letters*, 47(21), e2020GL090275. <https://doi.org/10.1029/2020GL090275>
- Chen, H., Gao, X. L., Lu, Q. M., & Wang, S. (2018). In situ observations of harmonic Alfvén waves and associated heavy ion heating. *The Astrophysical Journal*, 859(2), 120. <https://doi.org/10.3847/1538-4357/aabee2>
- Chen, H., Wang, X., Chen, L., Omura, Y., Tsurutani, B. T., Lin, Y., & Xia, Z. (2023). Evolution of chorus subpackets in the Earth's magnetosphere. *Geophysical Research Letters*, 50(21), e2023GL105938. <https://doi.org/10.1029/2023GL105938>
- Chen, H., Wang, X., Chen, L., Zhang, X.-J., Omura, Y., Chen, R., et al. (2024). Nonlinear electron trapping through cyclotron resonance in the formation of chorus subpackets. *Geophysical Research Letters*, 51(11), e2024GL109481. <https://doi.org/10.1029/2024GL109481>
- Chen, L., Thorne, R. M., Bortnik, J., & Zhang, X.-J. (2016). Nonresonant interactions of electromagnetic ion cyclotron waves with relativistic electrons. *Journal of Geophysical Research: Space Physics*, 121(10), 9913–9925. <https://doi.org/10.1002/2016JA022813>
- Chen, L., Zhu, H., & Zhang, X. (2019). Wavenumber analysis of EMIC waves. *Geophysical Research Letters*, 46(11), 5689–5697. <https://doi.org/10.1029/2019GL082686>
- Chu, X., Ma, D., Bortnik, J., Tobiska, W. K., Cruz, A., Bouwer, S. D., et al. (2021). Relativistic electron model in the outer radiation belt using a neural network approach. *Space Weather*, 19(12), e2021SW002808. <https://doi.org/10.1029/2021SW002808>
- Denton, R. E., Jordanova, V. K., & Fraser, B. J. (2014). Effect of spatial density variation and O<sup>+</sup> concentration on the growth and evolution of electromagnetic ion cyclotron waves. *Journal of Geophysical Research: Space Physics*, 119(10), 8372–8395. <https://doi.org/10.1002/2014JA020384>
- Denton, R. E., Menietti, J. D., Goldstein, J., Young, S. L., & Anderson, R. R. (2004). Electron density in the magnetosphere. *Journal of Geophysical Research*, 109(A9), A09215. <https://doi.org/10.1029/2003JA010245>
- Grach, V. S., & Demekhov, A. G. (2020). Precipitation of relativistic electrons under resonant interaction with electromagnetic ion cyclotron wave packets. *Journal of Geophysical Research: Space Physics*, 125(2), e2019JA027358. <https://doi.org/10.1029/2019JA027358>
- Green, J. C., & Kivelson, M. G. (2004). Relativistic electrons in the outer radiation belt: Differentiating between acceleration mechanisms. *Journal of Geophysical Research*, 109(A3), A03213. <https://doi.org/10.1029/2003JA010153>
- Horne, R. B., & Thorne, R. M. (1994). Convective instabilities of electromagnetic ion cyclotron waves in the outer magnetosphere. *Journal of Geophysical Research*, 99(A9), 17259–17273. <https://doi.org/10.1029/94JA01259>
- Kang, N., Lu, Q., Gao, X., Wang, X., Chen, H., & Wang, S. (2021). Propagation of electromagnetic ion cyclotron waves in a dipole magnetic field: A 2-D hybrid simulation. *Journal of Geophysical Research: Space Physics*, 126(12), e2021JA029720. <https://doi.org/10.1029/2021JA029720>
- Kessel, R. L., Fox, N. J., & Weiss, M. (2012). The radiation belt storm probes (RBSP) and space weather. *Space Science Reviews*, 179(1–4), 531–543. <https://doi.org/10.1007/s11214-012-9953-6>
- Kim, K.-H., Jun, C.-W., Kwon, J.-W., Lee, J., Shiokawa, K., Miyoshi, Y., et al. (2024). Observation and numerical simulation of cold ions energized by EMIC waves. *Journal of Geophysical Research: Space Physics*, 129(5), e2023JA032361. <https://doi.org/10.1029/2023JA032361>
- Kubota, Y., Omura, Y., & Summers, D. (2015). Relativistic electron precipitation induced by EMIC-triggered emissions in a dipole magnetosphere. *Journal of Geophysical Research: Space Physics*, 120(6), 4384–4399. <https://doi.org/10.1002/2015JA021017>
- Loto'aniu, T. M., Fraser, B. J., & Waters, C. L. (2009). The modulation of electromagnetic ion cyclotron waves by Pc 5 ULF waves. *Annales Geophysicae*, 27(1), 121–130. <https://doi.org/10.5194/angeo-27-121-2009>
- Meredith, N. P., Cayton, T. E., Cayton, M. D., & Horne, R. B. (2024). Strong relativistic electron flux events in GPS orbit. *Space Weather*, 22(12), e2024SW004042. <https://doi.org/10.1029/2024SW004042>
- Min, K., Lee, J., Keika, K., & Li, W. (2012). Global distribution of EMIC waves derived from THEMIS observations. *Journal of Geophysical Research*, 117(A5), A05219. <https://doi.org/10.1029/2012JA017515>
- Miyoshi, Y., Sakaguchi, K., Shiokawa, K., Evans, D., Albert, J., Conners, M., & Jordanova, V. (2008). Precipitation of radiation belt electrons by EMIC waves, observed from ground and space. *Geophysical Research Letters*, 35(23), L23101. <https://doi.org/10.1029/2008GL035727>
- Mursula, K., Bräysy, T., Niskala, K., & Russell, C. T. (2001). Pc1 pearls revisited: Structured electromagnetic ion cyclotron waves on Polar satellite and on ground. *Journal of Geophysical Research*, 106(A12), 29543–29553. <https://doi.org/10.1029/2000JA003044>
- Nakamura, S., Miyoshi, Y., Shiokawa, K., Omura, Y., Mitani, T., Takashima, T., et al. (2022). Simultaneous observations of EMIC-induced drifting electron holes (EDEHs) in the Earth's radiation belt by the Arase satellite, Van Allen Probes, and THEMIS. *Geophysical Research Letters*, 49(5), e2021GL095194. <https://doi.org/10.1029/2021GL095194>
- Nakamura, S., Omura, Y., & Angelopoulos, V. (2016). A statistical study of EMIC rising and falling tone emissions observed by THEMIS. *Journal of Geophysical Research: Space Physics*, 121(9), 8374–8391. <https://doi.org/10.1002/2016JA022353>
- Nakamura, S., Omura, Y., Shoji, M., Nose, M., Summers, D., & Angelopoulos, V. (2015). Subpacket structures in EMIC rising tone emissions observed by the THEMIS probes. *Journal of Geophysical Research: Space Physics*, 120(9), 7318–7330. <https://doi.org/10.1002/2014JA020764>
- Ojha, B., Omura, Y., Singh, S., & Lakhina, G. S. (2021). Multipoint analysis of source regions of EMIC waves and rapid growth of subpackets. *Journal of Geophysical Research: Space Physics*, 126(11), e2021JA029514. <https://doi.org/10.1029/2021JA029514>
- Omura, Y. (2021). Nonlinear wave growth theory of whistler-mode chorus and hiss emissions in the magnetosphere. *Earth Planets and Space*, 73(1), 95. <https://doi.org/10.1186/s40623-021-01380-w>
- Omura, Y., Pickett, J., Grison, B., Santolik, O., Dandouras, I., Engebretson, M., et al. (2010). Theory and observation of electromagnetic ion cyclotron triggered emissions in the magnetosphere. *Journal of Geophysical Research*, 115(A7), A07234. <https://doi.org/10.1029/2010JA015300>
- Omura, Y., & Zhao, Q. (2013). Relativistic electron microbursts due to nonlinear pitch angle scattering by EMIC triggered emissions. *Journal of Geophysical Research: Space Physics*, 118(8), 5008–5020. <https://doi.org/10.1002/jgra.50477>

- O'Neil, T. (1965). Collisionless damping of nonlinear plasma oscillations. *Physics of Fluids*, 8(12), 2255–2262. <https://doi.org/10.1063/1.1761193>
- Reeves, G. D., Spence, H. E., Henderson, M. G., Morley, S. K., Friedel, R. H. W., Funsten, H. O., et al. (2013). Electron acceleration in the Heart of the Van Allen radiation belts. *Science*, 341(6149), 991–994. <https://doi.org/10.1126/science.1237743>
- Santolík, O., Kletzing, C. A., Kurth, W. S., Hospodarsky, G. B., & Bounds, S. R. (2014). Fine structure of large-amplitude chorus wave packets. *Geophysical Research Letters*, 41(2), 293–299. <https://doi.org/10.1002/2013GL058889>
- Shoji, M., Miyoshi, Y., Katoh, Y., Keika, K., Angelopoulos, V., Kasahara, S., et al. (2017). Ion hole formation and nonlinear generation of electromagnetic ion cyclotron waves: THEMIS observations. *Geophysical Research Letters*, 44(17), 8730–8738. <https://doi.org/10.1002/2017GL074254>
- Shoji, M., & Omura, Y. (2013). Triggering process of electromagnetic ion cyclotron rising tone emissions in the inner magnetosphere. *Journal of Geophysical Research: Space Physics*, 118(9), 5553–5561. <https://doi.org/10.1002/jgra.50523>
- Shoji, M., & Omura, Y. (2017). Nonlinear generation mechanism of EMIC falling tone emissions. *Journal of Geophysical Research: Space Physics*, 122, 9924–9933. <https://doi.org/10.1002/2017JA023883>
- Summers, D., & Thorne, R. M. (2003). Relativistic electron pitch-angle scattering by electromagnetic ion cyclotron waves during geomagnetic storms. *Journal of Geophysical Research*, 108(A4), 1143. <https://doi.org/10.1029/2002JA009489>
- Terasawa, T., Hoshino, M., Sakai, J. I., & Hada, T. (1986). Decay instability of finite-amplitude circularly polarized Alfvén waves: A numerical simulation of stimulated Brillouin scattering. *Journal of Geophysical Research*, 91(A4), 4171–4187. <https://doi.org/10.1029/JA091iA04p04171>
- Tsurutani, B. T., Chen, R., Gao, X., Lu, Q., Pickett, J. S., Lakhina, G. S., et al. (2020). Lower-band “monochromatic” chorus riser subelement/wave packet observations. *Journal of Geophysical Research: Space Physics*, 125(10), e2020JA028090. <https://doi.org/10.1029/2020JA028090>
- Ukhorskiy, A. Y., Shprits, Y. Y., Anderson, B. J., Takahashi, K., & Thorne, R. M. (2010). Rapid scattering of radiation belt electrons by storm-time EMIC waves. *Geophysical Research Letters*, 37(9), L09101. <https://doi.org/10.1029/2010GL042906>
- Usanova, M. E., Mann, I. R., Bortnik, J., Shao, L., & Angelopoulos, V. (2012). THEMIS observations of electromagnetic ion cyclotron wave occurrence: Dependence on AE, SYMH, and solar wind dynamic pressure. *Journal of Geophysical Research*, 117(A10), A10218. <https://doi.org/10.1029/2012JA018049>
- Usanova, M. E., Mann, I. R., Kale, Z. C., Rae, I. J., Sydora, R. D., Sandanger, M., et al. (2010). Conjugate ground and multisatellite observations of compression-related EMIC Pc1 waves and associated proton precipitation. *Journal of Geophysical Research*, 115(A7), A07208. <https://doi.org/10.1029/2009JA014935>
- Wang, X., Chen, H., Omura, Y., Hsieh, Y.-K., Chen, L., Lin, Y., et al. (2024). Resonant electron signatures in the formation of chorus wave subpackets. *Geophysical Research Letters*, 51(8), e2023GL108000. <https://doi.org/10.1029/2023GL108000>
- Wang, Y., Li, Y., Liu, K., Song, W., Xiong, Y., & Yao, F. (2023). Statistical analysis of electromagnetic ion cyclotron rising-tone emissions based on deep learning. *Journal of Geophysical Research: Space Physics*, 128(5), e2022JA031085. <https://doi.org/10.1029/2022JA031085>
- Wygant, J. R., Bonnell, J. W., Goetz, K., Ergun, R. E., Mozer, F. S., Bale, S. D., et al. (2013). The electric field and waves instruments on the radiation belt storm probes mission. *Space Science Reviews*, 179(1–4), 183–220. <https://doi.org/10.1007/s11214-013-0013-7>
- Yue, C., Jun, C.-W., Bortnik, J., An, X., Ma, Q., Reeves, G. D., et al. (2019). The relationship between EMIC wave properties and proton distributions based on Van Allen probes observations. *Geophysical Research Letters*, 46(8), 4070–4078. <https://doi.org/10.1029/2019GL082633>
- Zenitani, S., & Nakano, S. (2023). Loading loss-cone distributions in particle simulations. *Journal of Geophysical Research: Space Physics*, 128(10), e2023JA031983. <https://doi.org/10.1029/2023JA031983>
- Zhang, X.-J., Mourenas, D., Artemyev, A. V., Angelopoulos, V., Kurth, W. S., Kletzing, C. A., & Hospodarsky, G. B. (2020). Rapid frequency variations within intense chorus wave packets. *Geophysical Research Letters*, 47(15), e2020GL088853. <https://doi.org/10.1029/2020GL088853>

## References From the Supporting Information

- Funsten, H. O., Skoug, R. M., Guthrie, A. A., MacDonald, E. A., Baldonado, J. R., Harper, R. W., et al. (2013). Helium, oxygen, proton, and electron (HOPE) mass spectrometer for the radiation belt storm probes mission. *Space Science Reviews*, 179(1–4), 423–484. <https://doi.org/10.1007/s11214-013-9968-7>